Korean J. Chem. Eng., 33(1), 107-113 (2016)
DOI: 10.1007/s11814-015-0098-7

pISSN: 0256-1115
eISSN: 1975-7220

Preparation of titanium dioxide/tungsten disulfide composite photocatalysts with enhanced photocatalytic activity under visible light

Lili Zheng, Weiping Zhang, and Xinyan Xiao†

School of Chemistry and Chemical Engineering, South China University of Technology, Guangzhou 510640, Guangdong, China
(*Received 2 December 2014 • accepted 12 May 2015*)

Abstract−Titanium dioxide/tungsten disulfide (TiO_2/WS_2) composite photocatalysts were fabricated *via* a one-step hydrothermal synthesis process, using $TiCl_4$ as titanium source and bulk WS_2 as sensitizer. The morphology, structure, specific surface area and optical absorption properties of the composite photocatalysts were characterized by scanning electron microscopy (SEM), transmission electron microscopy (TEM), Fourier transform infrared spectroscopy (FT-IR), X-ray powder diffraction (XRD), specific surface area analyzer and ultraviolet-visible diffuse reflection spectrum (UV-vis DRS), respectively. The photocatalytic activity of as-prepared photocatalysts was evaluated by the degradation of methyl orange (MO) under illumination of 500 W Xenon lamp. The results indicated that TiO_2/WS_2 composite photocatalysts possessed excellent photocatalytic activity, and ~95% of the degradation rate for MO was reached when molar ratio of WS_2 to TiO_2 was 0.004 and the irradiation time was 60 min. Moreover, the carrier trapping experiment and fluorescence spectra showed that $\bullet O_2^-$ was the key component in the photocatalytic degradation process and O_2 was reduced to be $\bullet O_2^-$ by the electrons from the conduction band of TiO_2 and WS_2 for the degradation of MO.

Keywords: TiO_2, Bulk WS_2, Visible-light, Methyl Orange, Photocatalytic Degradation Mechanism

INTRODUCTION

Various metal-oxide materials have been developed to solve some environmental pollution. Among various oxide semiconductor photocatalysts, titanium dioxide (TiO_2) has received much attention for degrading environmental contaminants because it is inexpensive, nontoxic, chemically stability and highly reactive [1]. However, it can only absorb ultraviolet light with wavelength less than 380 nm due to its wide band gap of 3.2 eV. To overcome the limitation of low efficiency in utilization of sunlight, numerous studies have been performed to extend the absorption band edge of TiO_2 into visible light region including metal ions doping [2] or non-metal ions doping [3], dye sensitization [4], deposition of noble-metal [5,6], semiconductor coupling TiO_2 and so on. Among these, numerous studies about using narrow band gap semiconductors to sensitize TiO_2 have been conducted for its advantage in maximum utilization of solar energy. There are two preconditions for narrow band gap semiconductors: (1) the band gap of the sensitizer should be near that of the optimum utilization of solar radiant energy; (2) and its energy level of conduction band should be higher than that of TiO_2 [7]. Certain metal sulfides with ideal optical properties and enough stability have been regarded as sensitizers to decorate TiO_2. Ho [8] reported the deposition of quantum sized WS_2 on the surface of TiO_2. Nanosized WS_2 made it possible to achieve electron transfer from WS_2 to TiO_2. Jang [9] fabricated CdS/TiO_2 nano-bulk composite by using TiO_2 to decorate bulk CdS with high crystalline and achieved efficient utilization of sunlight due to the ideal band gap energy and band positions of CdS. Hong [10] prepared ZnS-ZnO-CuS-CdS heterostructured photocatalyst with enhanced photocatalytic activity in degradation of methyl blue. However, there have been fewer investigations on using bulk WS_2 to directly sensitize TiO_2 nanoparticles.

Tungsten disulfide (WS_2) has been studied extensively recent years for its superior performance in resistance to acid/alkali and photocorrosion. And it was a layered semiconductor, in which the atoms in layers were covalently bound while atoms between adjacent layers interacted by weak van der Waals forces [11]. Although it is easy to excite bulk WS_2 for its narrow band gap of 1.35 eV by visible-light irradiation, the photoinduced electrons cannot effectively migrate to titanium dioxide because the conduction band edge of bulk WS_2 is lower than that of TiO_2. Fortunately, the quantum confinement effects make it possible to increase the band gap of nanosized WS_2 significantly, which achieves the transfer of electrons from the conduction band of WS_2 to that of TiO_2. Therefore, nanosized WS_2 can be regarded as an effective sensitizer to decorate high crystalline TiO_2 [7,8,12]. On the other hand, nanoparticles are inclined to agglomerate for its high surface activity in aqueous solution, resulting in reduced efficiency in the degradation of pollutant. It is also difficult to achieve industrial applications for the high cost in recycling nanoparticles. To improve the specific surface area of nanoparticles and reduce the agglomeration rate, researchers prefer to load TiO_2 nanoparticles on bulk materials such as activated carbon and zeolite.

We report here the fabrication of TiO_2/WS_2 composite photocatalysts via a one-step hydrothermal method. The formation of TiO_2/WS_2 composite promotes the separation rate of photoinduced

†To whom correspondence should be addressed.
E-mail: cexyxiao@scut.edu.cn

electron-hole pairs and increases the photocatalytic reactivity. In addition, the high stability and recyclable utilization of TiO_2/WS_2 composite photocatalysts make it possible to achieve industrial applications in environmental improvement. To evaluate the photocatalytic activity of the prepared photocatalysts, methyl orange was used as a probe chemical to be degraded under simulated sunlight irradiation.

EXPERIMENTAL

1. Materials

Titanium tetrachloride ($TiCl_4$, ≥99.0%, AR, Fuchen Chemical Reagent Co., China); tungsten disulfide (WS_2, 99%, Aladdin Reagent Co.); anhydrous ethanol (≥99.7%, AR, Nanjing Chemical Reagent Co., China); glycerol (≥99.0%, AR, Guangdong Xilong Chemical Co., China); sodium hexametaphosphate (AR, Tianjin Kermel Chemical Reagent Co., China); tertbutyl alcohol (TBA, CR, Shanghai Lingfeng Chemical Reagent Co., China); disodium ethylene diamine tetraacetate (Na_2-EDTA, ≥99.0%, AR, Shanghai Lingfeng Chemical Reagent Co., China); benzoquinone (BQ, ≥98.0%, CR, Sinopharm Chemical Reagent Co.,China); terephthalic acid (PTA, ≥99%, AR, Aladdin Reagent Co.); sodium hydroxide (NaOH, ≥96%, AR, Nanjing Chemical Reagent Co., China); methyl orange (MO, AR, Nanhua Chemical Reagent Co., China).

2. Synthesis of TiO_2/WS_2 Composite Photocatalyst

In this study, TiO_2/WS_2 composite photocatalysts with different amount of bulk WS_2 were prepared through hydrothermal method (Scheme 1(a)). The TiO_2/WS_2 precursor was achieved by the hydrolyzation of titanium tetrachloride ($TiCl_4$) and tungsten disulfide (WS_2) ethanol solution under ultrasonic vibration at ambient temperature. First, 4 mL $TiCl_4$ ethanol solution (2 M) and certain amount of bulk WS_2 were dispersed in 16 mL anhydrous ethanol. Then 5.6 mL solution composed of glycerol, sodium hexametaphosphate and deionized water was added into the above mixture dropwise under ultrasonic treatment for 10 min to promote the hydrolysis of $TiCl_4$ solution. The obtained TiO_2/WS_2 precursor was then transferred into 25 mL Teflon-lined stainless steel autoclave, followed by hydrothermal treatment at 413 K for 3 h in air atmosphere. After the autoclave was cooled naturally to room temperature, the samples were separated by centrifuge at 9,000 $r \cdot min^{-1}$ for 10 min, washed with anhydrous ethanol three times and dried at 353 K over 3 h. Finally, the samples were calcined at 773 K for 2 h to acquire TiO_2/WS_2 composite photocatalysts with excellent crystal structure.

The theoretical molar ratios of bulk WS_2 to $TiCl_4$ were controlled to be 0.002, 0.004, 0.008, 0.012, 0.016 and 0.02, respectively. TiO_2/WS_2 composite photocatalysts with different amount of bulk WS_2 were denoted as W-Ti-x (x=0.002, 0.004, 0.008, 0.012, 0.016 and 0.02, respectively). For comparison, TiO_2 photocatalyst was also prepared via a one-step hydrothermal method without the presence of bulk WS_2.

3. Characterization of TiO_2/WS_2 Composite Photocatalyst

FT-IR spectrum of the as-prepared samples were recorded on Bruker Tensor-27. XRD analysis was carried out at room temperature with a Bruker D8 Advance X-diffractometer using Cu Kα radiation (λ=1.5406 Å), operated at 40 kV and 40 mA, and a scanning speed of 5°/min in the 2θ range from 10° to 80°. The specific surface area was obtained by recording the N_2-absorption isotherm at the temperature of liquid nitrogen using a Beishide 3H-2000PS1 analyzer. The morphology of the samples was taken with a Hitachi S-3700N scanning electron microscope (SEM) attached to energy dispersive X-ray spectroscope (EDX) and JEOL JEM-2100P transmission electron microscope (TEM). UV-vis DRS was obtained by a Hitachi U-3010 spectrophotometer. The analysis range was from 800 to 300 nm, and $BaSO_4$ was used as a reflectance standard. UV-vis patterns were collected on a Shimadzu UV-2450 spectrophotometer. FL spectra were recorded on a JASCO FP-6500 type fluorescence spectrophotometer with 321 nm excitation source over a wavelength range from 300 to 600 nm. Photocatalytic degradation reaction was in a Nanjing Sidongke SGY-I multifunction photoreactor apparatus with 500 W Xenon lamp as simulated sunlight source.

4. Evaluation of Photocatalytic Activity

Photocatalytic activity of the as-prepared samples was evaluated by the degradation of MO under simulated sunlight irradiation in a photoreaction apparatus. A 500 W Xenon lamp was used as the light source to provide simulated sunlight. In each experiment, 50 mg TiO_2/WS_2 composite photocatalyst and 5 mg MO were dispersed in 250 mL deionized water. Prior to illumination, the sus-

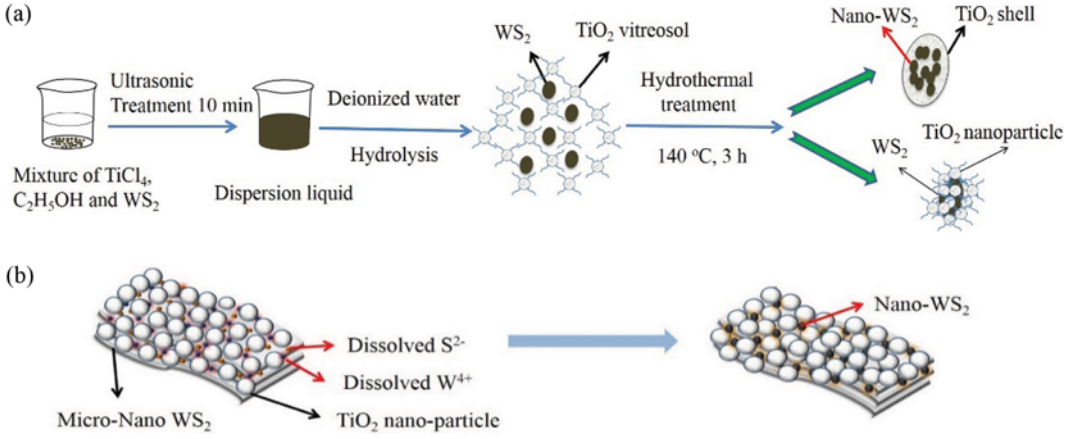

Scheme 1. (a), (b) Schematic diagram for the one-step synthesis of TiO_2/WS_2 composite photocatalysts.

pension was magnetically stirred in the dark for 30 min to reach adsorption-desorption equilibrium. Then the suspension was exposed to simulated sunlight irradiation, and 4 mL of suspension was collected with each irradiation time intervals of 10 min. The collected solution was centrifuged to isolate photocatalysts and analyzed with a UV-vis spectrophotometer. The degradation of MO was determined from its maximum absorption at a wavelength of 464 nm with deionized water as a reference sample and calculated according to Eq. (1):

$$D\% = \frac{A_0 - A_t}{A_0} \times 100\% \quad (1)$$

where D is degradation rate of MO, A_0 is the initial MO concentration and A_t is the MO concentration at certain reaction time t (min).

RESULTS AND DISCUSSION

1. Analysis of Morphology and Structure

FT-IR spectra of bulk WS_2, TiO_2 nanoparticles and TiO_2/WS_2 composite photocatalysts are shown in Fig. 1, in the wavenumber range from 4,000 to 400 cm^{-1}. The spectrum of TiO_2 nanoparticles revealed a broad band centered at 3,405 cm^{-1}, which can be assigned to -OH stretching vibration. An absorption peak observed at 1,635 cm^{-1} was attributed to the -OH bending mode of water adsorbed on the surface of TiO_2. And the broad peak observed in the range of 550-700 cm^{-1} indicated the existence of Ti-O bond [13]. Besides, the broad band at 1,035-1,125 cm^{-1} was attributed to the C-O vibration, which may have been caused by the organic residuals in the sample. CO_2 adsorbed on the metal cations may lead to the peak at 2,400 cm^{-1} [14]. The peak of -OH stretching vibration of absorbed water on the surface of TiO_2/WS_2 photocatalysts shifted towards the direction of larger wavenumber with the increasing amount of bulk WS_2. The result of FT-IR spectra indicated that TiO_2 and WS_2 coexisted in the prepared photocatalysts.

Fig. 2 shows the XRD patterns of TiO_2 nanoparticles, W-Ti-0.004 and W-Ti-0.02 composite photocatalysts. The analysis of diffraction peaks revealed that anatase phase was dominant in all samples, corresponding to the JCPDS card 21-1272. And the characteristic diffraction peaks of WS_2 (JCPDS card 08-0237) arose when the molar ratio of bulk WS_2 to TiO_2 equaled 0.004. However, the diffraction peak intensity of anatase phase gradually diminished, which may have been caused by the inhibition of WS_2 to the crystalline formation of TiO_2 [15,16]. The average crystalline grain size of the sample was determined by Scherrer's Eq. (2):

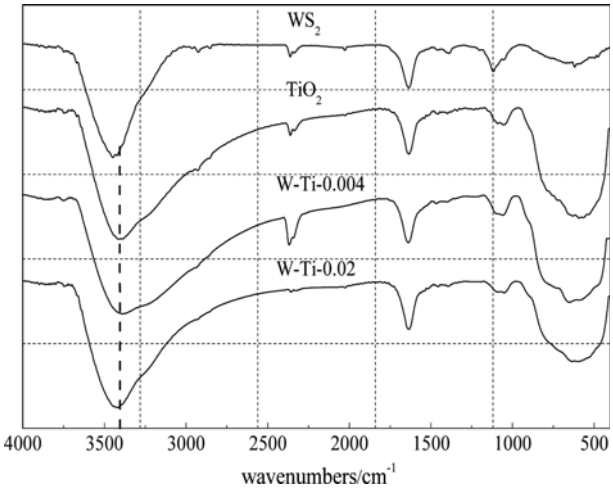

Fig. 1. FT-IR spectra of bulk WS_2, TiO_2 nanoparticles and TiO_2/WS_2 composite photocatalysts.

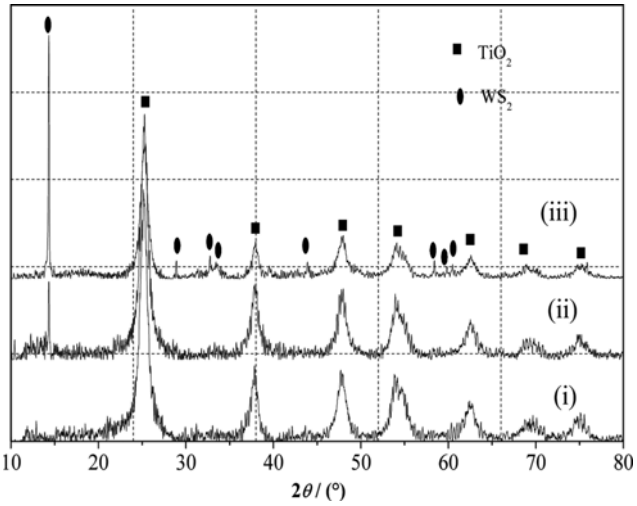

Fig. 2. XRD patterns of (i) TiO_2 nanoparticles; (ii) W-Ti-0.004 composite photocatalyst; (iii) W-Ti-0.02 composite photocatalyst.

Table 1. Comparison of average crystallite grain size and specific surface area of the samples derived from XRD and N_2-adsorption

Samples	Specific surface area/ $m^2 \cdot g^{-1}$	Average crystalline grain size/ nm
TiO_2	270.0	10.4
W-Ti-0.004	262.0	9.0
W-Ti-0.02	259.2	9.3

$$d = \frac{K\lambda}{\beta \cos\theta} \quad (2)$$

where d is the crystal size, λ is the wavelength of X-ray radiation (0.15418 Å), β is the full width at half-maximum, θ is the diffraction angle, and K is a constant (0.89).

Surface morphology analysis of W-Ti-0.004 composite photocatalyst has also been studied and its SEM and TEM images are shown in Fig. 3. Fig. 3(a) shows that the majority of bulk WS_2 was coated by TiO_2 nanoparticles with rough surface structure. And a small amount of bulk WS_2 appeared as a smooth surface without TiO_2 nanoparticles loading. Also, TiO_2 nanoparticles tightly were arranged on the bulk WS_2 surface and developed pore structure among nanoparticles, which was in favor of the adsorption and degradation of MO in photocatalyst system. Surface elemental analysis of the prepared photocatalysts (Fig. 3(a)) shows that the molar ratio of sulfur (S) element to tungsten (W) element approximately

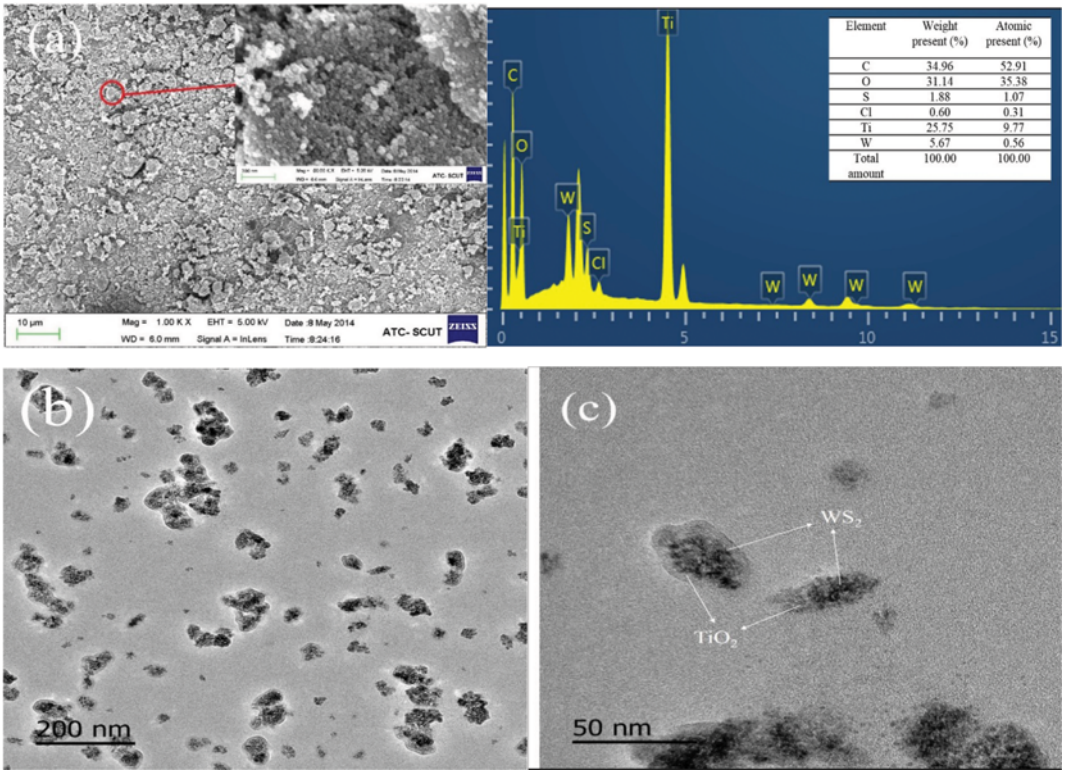

Fig. 3. SEM-EDS image (a), TEM images (b), (c) of W-Ti-0.004 composite photocatalyst.

equaled 2 : 1, proving that WS_2 and TiO_2 coexisted in the photocatalysts. Thus, it can be concluded that TiO_2 nanoparticles succeed in coating bulk WS_2 and forming TiO_2/WS_2 composite photocatalysts. Fig. 3(b) shows irregular nanoparticles and some of them are aggregated together. Certain nanoparticles exhibited core-shell structure, while others appeared to be nanocomposite morphology (Fig. 3(c)).

According to the above results, a probable schematic diagram for the growth of TiO_2/WS_2 composite is shown in Scheme 1. Under ultrasonic treatment, bulk WS_2 dispersed in TiO_2 vitreosol. And when the precursor of TiO_2/WS_2 was thermally treated at 140 °C for 3 h, the outer layer of bulk WS_2 produced W^{4+} and S^{2-} free ions (Scheme 1(b)) for the weak van der Waals forces between adjacent layers. Then, as the autoclave was naturally cooled to room temperature, W^{4+} recombined with S^{2-} resulting in the formation of WS_2 nanoparticles. Part of WS_2 nanoparticles were coated by TiO_2 nanoparticles, while some of them combined with TiO_2 nanoparticles and formed TiO_2/WS_2 nanocomposite, which greatly improved the photocatalytic activity (Scheme 1(a)).

2. Evaluation of Optical Absorption and Photocatalytic Activity

The characterization of optical absorption behavior played an important role in estimating photocatalytic performance of $TiO_2/$

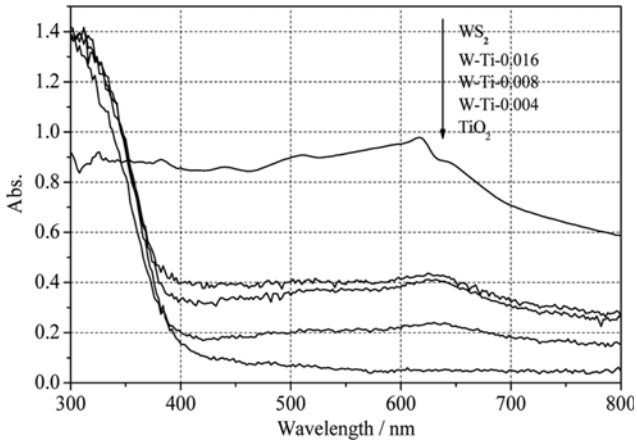

Fig. 4. UV-vis diffuse reflectance spectra of bulk WS_2, TiO_2 nanoparticles and TiO_2/WS_2 composite photocatalysts.

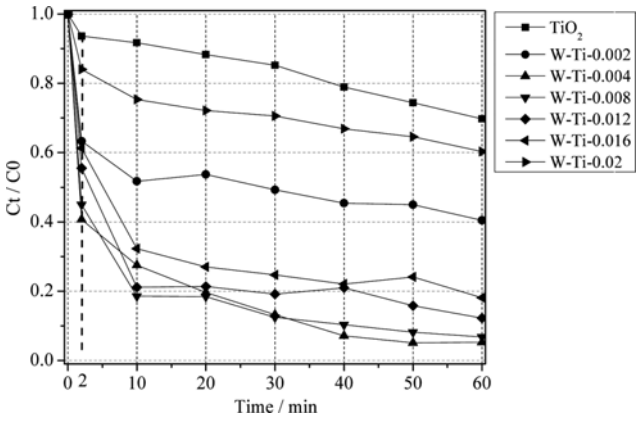

Fig. 5. Photocatalytic degradation curve of methyl orange catalyzed by TiO_2/WS_2 composite photocatalysts with different addition of bulk WS_2.

WS_2 composite photocatalysts. UV-vis DRS of bulk WS_2, TiO_2 nanoparticles and TiO_2/WS_2 composite photocatalysts are given in Fig. 4. It can be seen that TiO_2 nanoparticles exhibit strong absorption in UV region while almost had no absorption of visible light. Moreover, TiO_2/WS_2 composite photocatalysts achieved strong absorption in visible light region compared with TiO_2 nanoparticles.

To evaluate photocatalytic activity of TiO_2/WS_2 composite photocatalysts, degradation of MO was conducted under simulated sunlight irradiation. Fig. 5 shows the photocatalysis degradation curve of MO catalyzed by different photocatalysts under visible-light irradiation. It is obvious that the visible-light photocatalytic activity of TiO_2/WS_2 composite photocatalysts is superior to that of pure TiO_2. The degradation rate of MO was enhanced with the increase amount of bulk WS_2 loading and reached ~95% when the molar ratio of bulk WS_2 to TiO_2 equaled 0.004 after 60 min irradiation. However, the degradation rate of MO decreased when the amount of bulk WS_2 further increased. Such findings can be explained by the following points. (1) The addition of WS_2 reduced the agglomeration and stack of TiO_2 nanoparticles, promoting the uniform deposition of nanoparticle loading on the bulk WS_2 [17]. (2) The fabrication of TiO_2/WS_2 composite photocatalysts extended the absorption band edge to visible-light region and facilitated the separation of electron-hole pairs excited by simulated sunlight. (3) The excessive amount of bulk WS_2 addition lowered the permeability of the photocatalyst system and decreased the degradation rate of MO.

Fig. 6 reveals the UV-vis spectra of MO in W-Ti-0.004 photocatalyst system in function of time. Peaks at 464 nm and 276 nm in MO solution correspond to the azo bond and the phenyl ring, respectively [18]. MO absorbed on the surface of photocatalysts was degraded to hydrazine under illumination, which led to the emergence of the absorption peak at 245 nm and the decrease of absorption peak at 464 nm [19]. The competitive photocatalytic degradation of hydrazine and MO resulted in the lower degradation rate of MO at 10-60 min. When the MO was nearly decomposed after irradiation for 60 min, the content of hydrazine was also at a relatively low level, which indicated that the prepared photocatalysts had excellent photocatalytic activity.

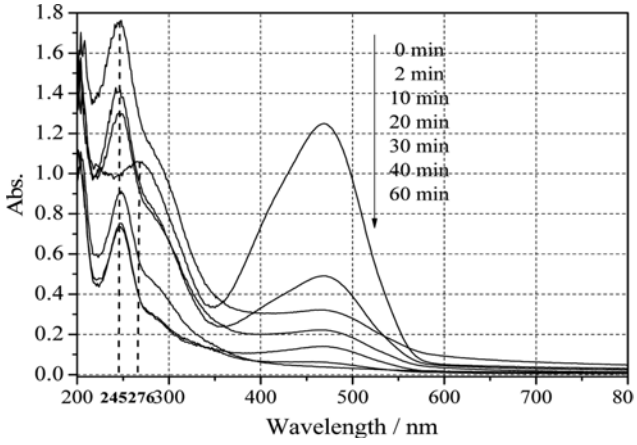

Fig. 6. UV-vis spectra of MO in W-Ti-0.004 photocatalysis system in function of time.

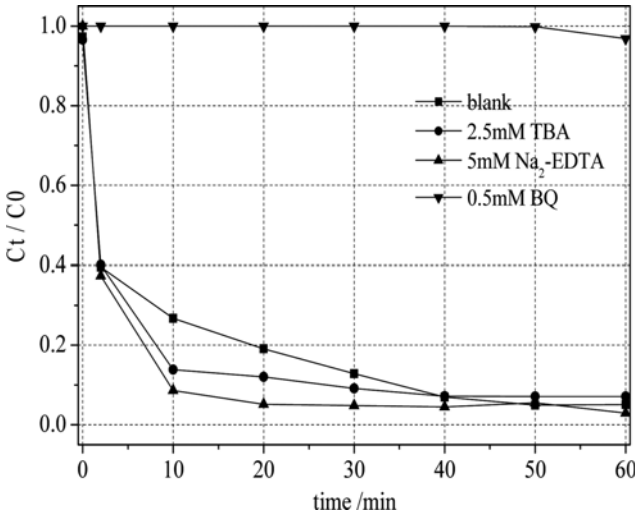

Fig. 7. Effect of photogenerated carrier trapping agent on degradation of methyl orange over W-Ti-0.004 composite photocatalyst.

3. Carrier Trapping Experiments and Photocatalytic Degradation Mechanism

Various primary reactive species, including hydroxyl radical (•OH), photo-generated hole (h^+), superoxide radical ($\bullet O_2^-$) could be formed during the photocatalytic degradation process [20]. Scavenger experiments were conducted to study the main reactive species in photocatalytic degradation process and the photocatalytic degradation mechanism of TiO_2/WS_2 composite photocatalysts [20]. Herein, tertbutyl alcohol (TBA), disodium ethylene diamine tetraacetate (Na_2-EDTA) and benzoquinone (BQ) were used as •OH, h^+ and $\bullet O_2^-$ scavenger, respectively [21]. Fig. 7 shows the influence of TBA, Na_2-EDTA and BQ on photocatalytic degradation rate of MO. The addition of TBA or Na_2-EDTA accelerated the degradation rate of MO to some extent, while the presence of BQ inhibited the photocatalytic degradation of MO significantly compared with system of W-Ti-0.004 photocatalyst without scavenger. Therefore, $\bullet O_2^-$ played the most important role in photocatalytic degradation of MO and the trapping of h^+ and •OH directly or indirectly promoted the separation of photogenerated hole-electron pairs leading to the efficient degradation of MO.

To further analyze the photocatalytic degradation mechanism, fluorescence technique was adopted to determine •OH. Terephthalic acid (PTA) was used to react with •OH radicals to produce 2-hydroxyterephthalic acid (PTAOH) in aqueous solution [21]. PTAOH is a highly fluorescent substance and its fluorescence emission spectra are excited at 321 nm from TA solution including 50 mg W-Ti-0.004 photocatalysts and certain amount of carrier trapping agent. Fig. 8 shows the fluorescence spectrum in function of reaction time observed at 426 nm for various photocatalyst systems. In the presence of BQ, the W-Ti-0.004 photocatalyst system shows weak fluorescence intensity, indicating that the majority of •OH was formed by the reaction among $\bullet O_2^-$, H^+ and e^-. And both of WS_2 and TiO_2 nanoparticles can provide a sufficient potential to reduce O_2 to $\bullet O_2^-$ through the one-electron reduction process [21] and further generated •OH (Eqs. (3)-(4)).

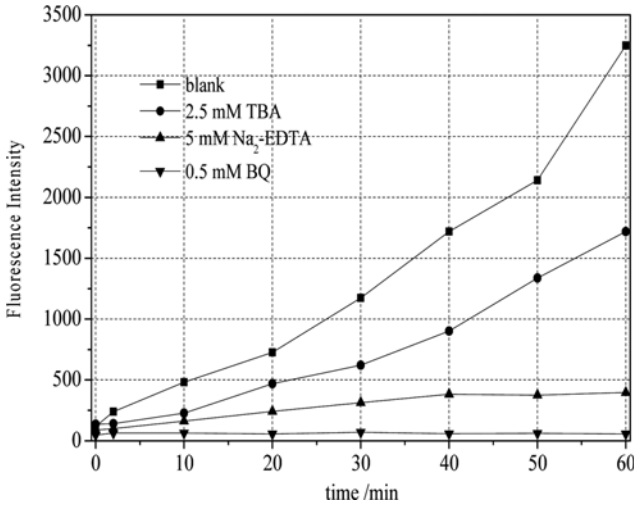

Fig. 8. Fluorescence spectra of hydroxyl radicals at 426 nm in W-Ti-0.004 photocatalysis system under different carrier trapping agent.

$$\bullet O_2^- + 2H^+ + e^- \text{ (CB)} \rightarrow H_2O_2 \quad (3)$$

$$H_2O_2 \rightarrow 2 \bullet OH \quad (4)$$

Na_2-EDTA capturing h^+ in W-Ti-0.004 photocatalyst system led to lower fluorescence intensity. It may be attributed to the fact that a small amount of •OH was generated by the reaction between H_2O and h^+. Thus, the capture of h^+ indirectly reduced the amount of •OH in photocatalysis system.

According to the results of the scavenger experiments and fluorescence spectra, a possible reaction mechanism is illustrated in Scheme 2. First, TiO_2/WS_2 composite photocatalysts absorbed a certain amount of MO to build adsorption-desorption equilibrium in the dark. Then TiO_2/WS_2 composite photocatalyst was excited by simulated sunlight illumination to generate electron-hole pairs. Due to the higher E_{VB} values of TiO_2 nanoparticles, the photoinduced holes easily migrated to the valence band of bulk WS_2 while some holes oxidized H_2O to •OH. Simultaneously, the electrons on the conduction band of WS_2 moved towards the conduction band of TiO_2 nanoparticles and reduced the absorbed oxygen to produce superoxygen anionic free radicals ($\bullet O_2^-$) that was the main reactive radical species to degrade MO (Eqs. (5)-(8)) [8].

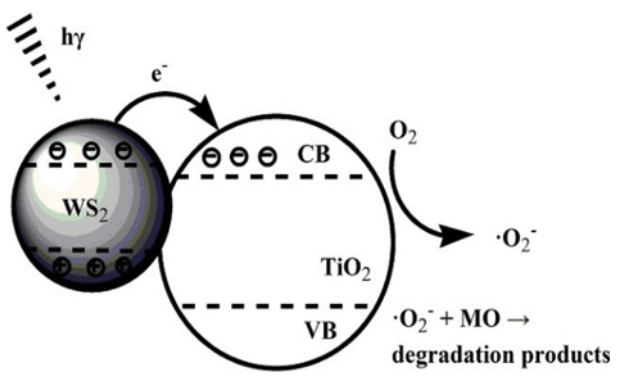

Scheme 2. The proposed photodegradation process on W-Ti-0.004 composite photocatalyst.

$$TiO_2/WS_2 + h\gamma \rightarrow TiO_2/WS_2\ (h^+ + e^-) \quad (5)$$

$$e^- \text{ (CB)} + O_2 \rightarrow \bullet O_2^- \quad (6)$$

$$h^+ + H_2O \rightarrow \bullet OH + H^+ \quad (7)$$

$$\bullet O_2^- + MO \rightarrow \ldots \rightarrow \text{degradation products} \quad (8)$$

CONCLUSIONS

TiO_2/WS_2 composite photocatalysts were prepared *via* a one-step hydrothermal method. Narrow band gap of bulk WS_2 enhanced the visible-light absorption of the prepared photocatalysts. The formation of TiO_2/WS_2 composite under hydrothermal condition promoted the separation of the photoinduced electron-hole pairs to facilitate the photocatalytic degradation of MO. The degradation rate of MO under visible-light illumination reached ~95.0% in 60 min when the molar ratio of WS_2 to TiO_2 was 0.004. The results of scavenger experiments and fluorescence spectra showed that the formed TiO_2/WS_2 composite supported on bulk WS_2 provided electrons to reduce adsorbed oxygen, and the produced superoxygen anionic free radicals ($\bullet O_2^-$) played the key role in the degradation of MO.

ACKNOWLEDGEMENTS

This work was supported by the National Natural Science Foundation of China (21376099).

REFERENCES

1. W. S. Zhu, Y. H. Xu, H. M. Li, B. L. Dai, H. Xu, C. Wang, Y. H. Chao and H. Liu, *Korean J. Chem. Eng.*, **31**, 2 (2014).
2. Y. Zhao, C. Z. Li, X. H. Liu, F. Gu, H. L. Du and L. Y. Shi, *Appl. Catal. B-Environ.*, **79**, 208 (2008).
3. A. N. Kadam, R. S. Dhabbe, M. R. Kokate, Y. B. Gaikwad and K. M. Garadkar, *Spectrochim. Acta. A*, **133**, 669 (2014).
4. G. H. Qin, Y. Zhang, X. B. Ke, X. L. Tong, Z. Sun, M. Liang and S. Xue, *Appl. Catal. B-Environ.*, **129**, 599 (2013).
5. X. F. Zhou, J. Lu, J. L. Cao, M. F. Xu and Z. S. Wang, *Ceram. Int.*, **40**, 3975 (2014).
6. A. Mahmood and S. I. Woo, *Korean J. Chem. Eng.*, **30**, 10 (2013).
7. D. W. Jing and L. J. Guo, *Catal. Commun.*, **8**, 795 (2007).
8. W. K. Ho, J. C. Yu, J. Lin, J. G. Yu and P. S. Li, *Langmuir*, **20**, 5865 (2004).
9. J. S. Jang, W. Li, S. H. Oh and J. S. Lee, *Chem. Phys. Lett.*, **425**, 278 (2006).
10. E. Hong, T. Choi and J. H. Kim, *Korean J. Chem. Eng.*, **32**, 3 (2015).
11. M. Thomalla and H. Tributsch, *J. Phys. Chem. B*, **110**, 12167 (2006).
12. S. Jana, P. Bera, B. Chakraborty, B. C. Mitra and A. Mondal, *Appl. Surf. Sci.*, **317**, 154 (2014).
13. M. B. Suwarnkar, R. S. Dhabbe, A. N. Kadam and K. M. Garadkar, *Ceram. Int.*, **40**, 5489 (2014).
14. J. Kaur and S. Singhal, *Ceram. Int.*, **40**, 7417 (2014).
15. S. K. Leghari, S. Sajjad, F. Chen and J. L. Zhang, Chem. Eng. J., **166**, 906 (2011).

16. S. S. Liu, J. F. Huang, L. Y. Cao, J. Y. Li, H. B. Ouyang, X. W. Tao and C. Liu, *Mat. Sci. Semicon. Proc.*, **25**, 106 (2014).
17. T. D. N. Phan, V. H. Pham, J. S. Chung, M. Chhowalla, T. Asefa, W. J. Kim and E. W. Shin, *Appl. Cata. A-Gen.*, **473**, 21 (2014).
18. D. Y. Xu, F. Cheng, Q. Z. Lu and P. Dai, *Ind. Eng. Chem. Res.*, **53**, 2625 (2014).
19. W. J. Li, D. Z. Li, J. J. Xian, W. Chen, Y. Hu, Y. Shao and X. Z. Fu, *J. Phys. Chem. C*, **114**, 21482 (2010).
20. W. H. Liu, Q. Z. Hu, F. Mo, J. J. Hu, Y. Feng, H. W. Tang, H. N. Ye and S. Miao, *J. Mol. Catal. A-Chem.*, **395**, 322 (2014).
21. J. Cao, B. D. Luo, H. L. Lin, B. Y. Xu and S. F. Chen, *J. Hazard. Mater.*, **217**, 107 (2012).